Available online at www.sciencedirect.com

ScienceDirect

Materials Today: Proceedings 4 (2017) S253–S262

materialstoday: PROCEEDINGS

www.materialstoday.com/proceedings

NRW 2016

Polyol synthesized aluminum doped zinc oxide nanoparticles - influence of the hydration ratio on crystal growth, dopant incorporation and electrical properties☆

Thomas Straube[a,b], Jürgen Linders[b], Thomas Mayer-Gall[a,b], Torsten Textor[c], Christian Mayer[b], Jochen S. Gutmann[a,b]*

[a]*Deutsches Textilforschungszentrum Nord-West gGmbH, Krefeld, Germany*
[b]*Institute of Physical Chemistry and Center for Nano Integration, Duisburg-Essen, Germany*
[c]*Reutlingen University, Textile and Design, Reutlingen, Germany*

Abstract

The wet chemical deposition of solution processed transparent conducting oxides (TCO) provides an alternative low cost and economical deposition technique to realize large-areas of conducting films. Since the price for the most common TCO Indium Tin Oxide rises enormously, Aluminum Zinc Oxide (AZO) as alternative TCO reaches more and more interest. The optoelectronical properties of nanoparticle coatings strongly depend beneath the porosity of the coating on the shape and size of the used particles. By using bigger or rod-shaped particles it is possible to minimize the amount of grain boundaries resulting in an improvement of the electrical properties, whereas particles bigger than 100 nm should not be used if highly transparent coatings are necessary as these big particles scatter the visible light and lower the transmittance of the coatings. In this work we present a simple method to synthesize AZO particles with different shape and size, but comparable electronical properties. We use a simple, well reproducible polyol method for synthesis and influence the shape and size of the particles by adding different amounts of water to the precursor solution. We can show that the addition of aluminum as dopant strongly hinders the crystal growth but the addition of water counteracts this, so that both, spherical and rod-shaped particles can be obtained.

Selection and Peer-review under responsibility of 7th North Rhine-Westphalian Nano-Conference.

Keywords: Aluminum Zinc Oxide, AZO, Nanoparticles, Polyol process, ^{27}Al-NMR, Crystal Growth, Conductivity

* Corresponding author. Tel.: +49 2151-843-2010; fax: +49 2151-843-2095.
E-mail address: jochen.gutmann@dtnw.de

Selection and Peer-review under responsibility of 7th North Rhine-Westphalian Nano-Conference.

1. Introduction

Transparent Conducting Oxides (TCO) are used for a wide range of optoelectronic applications, because thin films of TCO materials combine the unique properties as high transmittance in the visible region and high electrical conductivity. Since the price for the most commonly used TCO Indium Tin Oxide (ITO) rises enormously due to a rapidly growing demand and rare earth abundance of Indium, a cost effective alternative with comparable quality is needed. Aluminum Zinc Oxide (AZO) as alternative TCO reaches the most interest, because the precursors are nontoxic, cheap and earth-abundant [1,2,3]. There are diverse established physical and chemical techniques as sputtering, evaporation, pulsed laser deposition, chemical vapour deposition or sol-gel technique to deposit thin TCO films directly on substrate [4,5]. Coatings prepared by these techniques are highly transparent and exhibit the best electrical properties reported [6,7] but suffer from different drawbacks as high costs for vacuum processing, the limitation to flat and mostly heat stable substrates and the difficulty to scale up the processes on large areas. An alternative low cost and economical deposition technique is the wet chemical deposition of nanoparticle suspensions. The advantage of this approach is to separate the step of TCO synthesis from the step of deposition on the substrate, so that a low temperature deposition of conductive particle layer on different substrates can be put into practice [8,9]. The disadvantage of this approach is, that the resistances of particle coatings are higher than those of coatings prepared by conventional deposition techniques [6]. That can be ascribed to higher porosities (lower density) and a big amount of grain boundaries that hinder the electron transfer from particle to particle and therefore through the coating [10,11,12,13]. To prepare particle coatings with adequate properties, stable nanoparticle dispersions or inks with low-agglomerated, conductive nanoparticles are necessary [14,15]. With the help of crystalline solution processed nanoparticles and different additives and stabilizers it is possible to prepare low agglomerated particle suspensions to guarantee a good arrangement of the particles on a substrate [16,17]. Beneath the porosity, the shape and size of the nanoparticles can have a big impact on the coating's properties. By using bigger particles it is possible to minimize the amount of grain boundaries resulting in an improvement of the electrical properties [13,18,19], whereas particles bigger than 100 nm should not be used if highly transparent coatings are necessary as these big particles scatter the visible light and lower the transmittance of the coatings [11]. All in all, particle coatings with high transparency and good electrical properties can be achieved using particles of sufficiently small size and good conductivity which can be dispersed free of agglomerates.

In this work we concentrate on the synthesis of highly crystalline spherical and rod-shaped Aluminum-doped Zinc Oxide nanocrystals using a simple polyol method. To control the shape of the nanoparticles we add different amounts of water to the precursor solution as described by Lee et al. [19] who obtained spherical and rod-shaped ZnO nanoparticles using this method. We investigate the influence of the hydration ratio and the dopant on the crystal-size and shape by X-ray powder diffraction (PXRD) analysis and scanning electron microscopy (SEM) and the electrical properties by resistance measurements of the bulk material. With the help of ^{27}Al-MAS-NMR experiments and elemental analysis (ICP-OES), we investigate the incorporation of aluminum in zinc oxide.

2. Materials and Methods

2.1. Synthesis of AZO nanoparticles

Syntheses were carried out in a high-pressure reactor (Berghof) with a teflon vessel of 500 ml volume and an agitator. Zinc acetate dehydrate ($Zn(CH_3COO)_2$, >95%, Roth) and aluminium nitrate nonahydrate ($Al(NO_3)_3\,x9H_2O$, ≥98%, Roth) were used as precursors and diethylene glycol (DEG, ≥99%, Merck) with an estimated water content of 0.3 wt.% as solvent. All samples were synthesized with a total precursor amount of 0.255 mol/l, a volume of 200 ml DEG and a dopant degree of 2 at.% aluminum, whereas the dopant degree was defined as the molar ratio of the metal ions of the precursors [$n(AL^{3+})$ / $n(Al^{3+}+Zn^{2+})$]x100%. To investigate the influence of the hydration ratio different amounts of deionized water (DI) were added to 200 ml solvent DEG. The hydration ratio "h" is defined as the molar ratio of the total water content to the total amount of the precursor ions, $h= n(H_2O_{total}) / n(Zn^{2+}+Al^{3+})$, with $n(H_2O_{total})=n(H_2O_{DEG})+n(H_2O_{Al\text{-}nitrate})+n(H_2O_{DI})$. We synthesized samples with h=0.9, 2, 3, 6, 12 and for comparison undoped ZnO nanoparticles with a hydration ratio of about h=2.7 using 0.25 mol/l zinc acetate dihydrate as precursor. For synthesis, precursors, solvent and additional water were filled into the teflon vessel and to guarantee a

constant composition of the atmosphere over the reaction solution, the reactor chamber was purged with argon as inert gas for several minutes. To avoid deformation of the teflon vessel while synthesis, the reactor chamber was filled with an overpressure of 10 bar argon. Before heating up the solution to 200°C for 8 h, the agitator was started to stir continuously at 250 rpm. After synthesis, the reactor cooled down to room temperature and the obtained particles were centrifuged and washed several times with ethanol before the particles were dried in an oven at 80°C over night.

2.2. Characterization of AZO nanoparticles

Scanning electron microscopy (SEM) of diluted particles on carbon templates was carried out with an S3400N from Hitachi. *X-ray powder diffraction (PXRD)* was carried out with a powder diffractometer Bruker D8 Advance in Bragg-Brentano geometry with Cu-Kα radiation (1.54 Å; 40 kV and 40 mA) in a 2 theta range from 5-90°. *^{27}Al MAS NMR* experiments were performed on a Bruker ASX 400 spectrometer with a 104.261 MHz resonance frequency for aluminum nuclei. For all solid-state spectra, magic angle spinning (MAS) was applied at frequencies of 14500 Hz in a 4 mm rotor and the excitation of ^{27}Al nuclei was induced by a single 90° pulse of 5.75 µs duration. Generally, the fully decoupled free induction decay was accumulated over 20k scans and fourier-transformed in order to obtain the spectrum. To allow for full spin-lattice relaxation a waiting period of 3 s was used between the experiments. All experiments were carried out at ambient temperature (298 K). *Quantitative elemental analyses* were performed by inductively coupled plasma optical emission spectrometry (ICP-OES) with a Varian 720-ES-OES. For that a small amount of AZO powders were diluted with nitric-acid (69%, Roth) and solved by microwave-digestion. *Resistivity measurements* of powders were performed by a two-point measurement system. For that 0.3 grams of pestled powder were filled between two hardened stainless steel cylinders with a diameter of 13 mm as known from common KBr-presses. The measurements were performed for 50 seconds with a pressure of 3.7×10^3 bar at a constant current with a Multimeter (Keithley), whereas the pressure was applied by automatically compacting the powders in an uniaxial press (Hydraulic Power Press, Specac). The results were calculated from the average resistance measured in 50 seconds. The thickness of the pellets and the specific resistance of the powders were calculated based on the pressed powder mass, the density for crystalline ZnO (5.6 $g \cdot cm^{-3}$) and the diameter of the used cylinder for pellet preparation.

3. Results and Discussion

3.1. Influence of the hydration ratio and aluminum doping on the particle morphology and crystal growth

After the synthesized particles were washed several times with ethanol, a small amount of selected particles were diluted with Ethanol and placed on carbon planchets. After drying in air over night, SEM photographs of the obtained particles were taken. The following micrographs in figure 1 illustrate undoped ZnO and AZO particles synthesized with a hydration ratio “h” of h=0.9, 3 and 12. It is obvious that the shape and size for the different AZO particles differ. AZO particles synthesized with the lowest hydration ratio (h=0.9) are strongly agglomerated but some small isolated particles can be seen in the background. The particles of undoped ZnO and AZO h=3 and h=12 are not strongly agglomerated and differ in size and shape. The AZO particles of h=3 are small and spherical, whereas AZO particles of h=12 and undoped ZnO particles are bigger and more like rod-shaped particles.

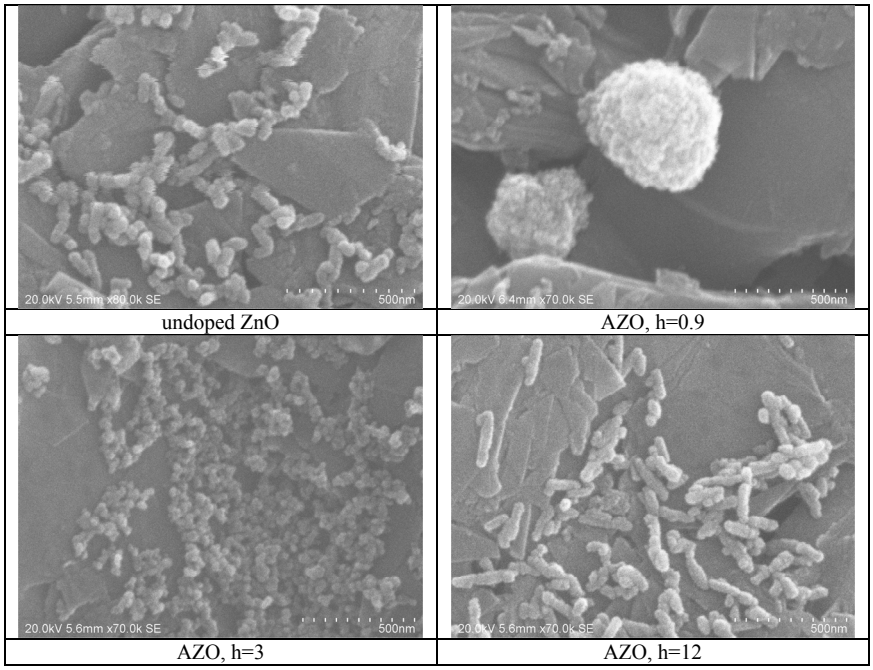

Fig. 1. SEM micrographs of undoped ZnO and AZO particles synthesized at different hydration ratios (h=0.9, 3, 12).

To investigate the crystallinity of the obtained particles we performed PXRD analysis of powders. Figure 2 (left) shows the XRD patterns for the synthesized ZnO and AZO particles. The XRD pattern for ZnO as well as for AZO correspond to the crystalline hexagonal-wurtzite-structure of ZnO which was identified by comparison with the spectra from JCPDS (Card No. 36-1451). Furthermore for AZO particles no phases of any aluminium oxide species were detected. Nevertheless, both the hydration ratio and the doping with aluminum strongly influence the peak width and the relative peak intensities.

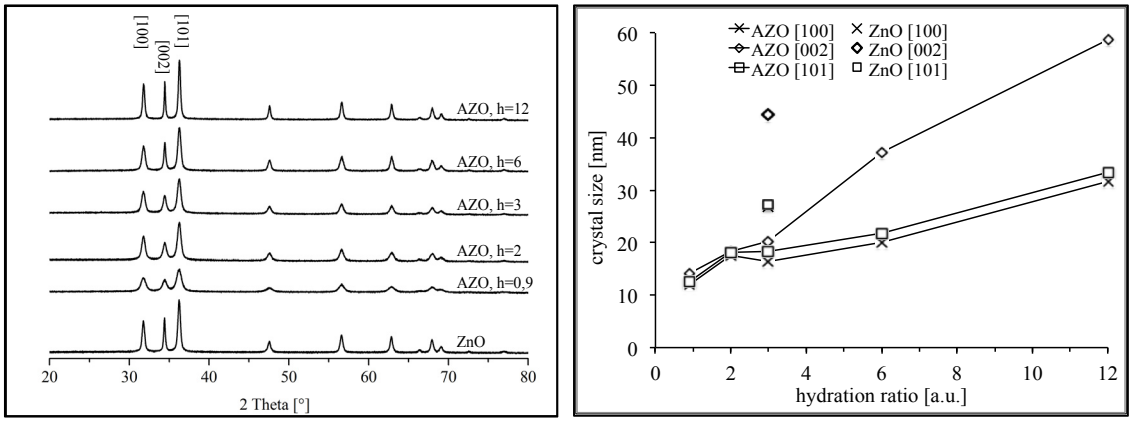

Fig. 2. left: XRD pattern for ZnO und AZO powders synthesized at different hydration ratio (h);
right: crystal-size calculated for three different Bragg reflexes in dependence of the hydration ratio.

The peak width of the Bragg reflexes decreases and the relative intensities increase with increasing hydration ratio what can be assigned to an improved crystallinity. Using the Scherrer's equation the crystallite size for the most intensive Bragg peaks [100], [002] and [101] were calculated and plotted against the hydration ratio (Figure 2, right). With increasing hydration ratio the crystallite-size increases. For h=0.9 the crystal size of the peaks [100], [002] and

[101] is about 12, 14 and 13 nm, for h=12 its about 32, 59 and 33 nm. Furthermore it's quite evident that the relative peak intensity ratio of I_{002}/I_{100} differs. For h=0.9, 2 and 3 these ratios are in a range from 0.8-0.86 and for h=6 and 12 about 1 and 1.1. The different aspect ratios stand for varying particle morphologies. With increasing hydration ratio the particles change their form from spherical to rod-shaped particles. *Lee et al.* [19] investigated the influence of the hydration ratio on the particle growth of polyol synthesized undoped ZnO particles and also observed a rod-shaped growth for ZnO particles with increasing hydration ratio. They developed a reaction mechanism for the water mediated growth and explain that the hydration ratio mediated particle-growth in ZnO is based on the fact that water acts both as reactant and as product of the hydrolysis and condensation reaction for the oxide formation and affects the kinetics of the nucleation and growth process, as well as *Poul et al.* [20] generally describe. Although we investigate the influence of the growth of AZO particles in dependence of the hydration ratio, our findings fit well with the findings of *Lee et al.* for undoped ZnO. But if we compare the crystal structure of undoped ZnO particles with AZO for nearly the same hydration ratio, it becomes obvious, that beneath the hydration ratio, the introduction of aluminum strongly affects the crystallinity and the particle morphology. The crystal-sizes of undoped ZnO particles for the peaks [100], [002] and [101] were calculated with 27, 44 and 27 nm and are with an aspect ratio I_{002}/I_{100} of 0.98 rod-shaped. The obtained AZO particles for h=3 are with 16, 20 and 18 nm for the same peaks smaller and with an aspect ratio I_{002}/I_{100} of 0.86 spherical grown. Consequently, doping with aluminum strongly hinders the particle growth, especially the growth for the [002] plane. The incorporation of dopant atoms generally hinders the particle growth and decrease the crystallinity [21,22] but here we can show that an increase of the water content reduces the influence of the dopant on the crystal-growth, so that rod-shaped AZO particles with improved crystallinity can be synthesized.

3.2. Incorporation of aluminum in ZnO and electrical properties of AZO particles

To investigate the influence of the hydration ratio on the incorporation of aluminum in ZnO we firstly determined the chemical composition of the synthesized AZO particles by ICP-OES to get general information about the aluminum content in the powders. Independent from the hydration ratio the initially inserted aluminum concentration of 2 at.% could be found within the limits of the standard deviation (Table 1).

Table 1: chemical composition of the AZO particles measured by ICP-OES

Sample	measured Al content [at.%]
AZO, h=0.9	1.98 ± 0.09
AZO, h=2	2.23 ± 0.47
AZO, h=3	2.10 ± 0.10
AZO, h=6	2.20 ± 0.09
AZO, h=12	2.26 ± 0.09

It is known that aluminum ions can occupy different lattice sites in the wurtzite-structure of ZnO what makes the dopant mechanism very complex. By ^{27}Al-nuclear magnetic resonance spectroscopy (^{27}Al-NMR) the distribution of the aluminum atoms in the host lattice of ZnO can be depicted and characterized [23,24,25,26,27,28]. Related to the crystallographic composition of the wurtzite-structured zinc oxide, different lattice sites can be occupied by the dopant. Al^{3+} ions can either substitute Zn^{2+} ions in a tetrahedral coordination with four oxygen atoms ($Al4_{sub}$) or situate on interstitial lattice sites and can be tetrahedrally ($Al4_{int}$) or octahedrally ($Al6_{int}$) coordinated by four or six oxygen atoms as e.g. *Kelchtermans et al.* [26] describe. Beneath these positions, Al^{3+} ions can be pentahedral coordinated [23,27], whereas this coordination generally can not be dedicated as a convenient position in the lattice of the ZnO but is known from ^{27}Al-NMR investigations of different aluminium oxide structures and were often found at the surface of the solids bound to different organic molecules [29,30,31]. *Avadhut et al.* [25] performed multinuclear (^{1}H, ^{13}C, ^{27}Al) spectroscopic analysis with the aim to localize the different Al species in AZO. They found Al6, Al5 and Al4 in a disordered, amorphous environment and localized these species near the surface of

AZO particles bound to organic molecules as solvent, salt or adsorbed water and just $Al4_{sub}$ with a small amount of about 0.1 at.% in an ordered, crystalline environment. Further they correlated their findings with the electrical properties and showed that Al6, Al5 and Al4 behave as insulating particle shell that results in a decrease of the conductivity due to electron trapping and that only $Al4_{sub}$ causes an increase of the conductivity by n-doping. We performed ^{27}Al-NMR experiments to get a deeper insight on the distribution and solubility of aluminum in the host lattice of ZnO in dependence of the hydration ratio. In Figure 3, left, the ^{27}Al-NMR spectra for AZO in dependence of the hydration ratio are shown and the dotted lines mark the chemical shift values for the different Al^{3+} species known from literature.

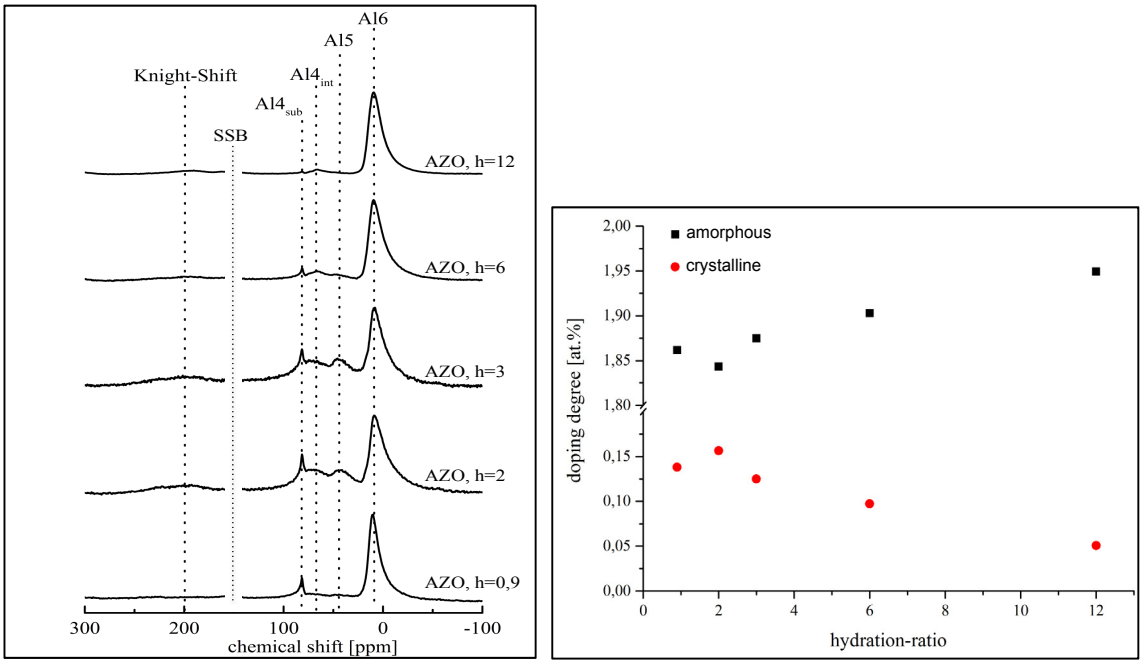

Fig. 3. left: ^{27}Al-NMR spectra of AZO synthesized with different hydration ratio and dotted lines that mark the chemical shift values for the known peaks; right: calculated amount of amorphous and crystalline coordinated aluminum in dependence of the hydration ratio.

For all ^{27}Al-NMR spectra Al6 is the dominating species whereas the other Al species can be recognized as well. It is obvious that the peaks for Al6, Al5 and $Al4_{int}$ are very broad in contrast to $Al4_{sub}$ what indicates that $Al4_{sub}$ is located in a highly ordered, crystalline environment and Al6, Al5 and $Al4_{int}$ in a disordered, amorphous environment [20-22]. A change of the peak intensities in dependence of the hydration ratio is noticeable. With increasing hydration ratio the intensity for Al6, Al5 and $Al4_{int}$ increase related the peak for $Al4_{sub}$. To estimate the relative change of amorphous (Al6, Al5, $Al4_{int}$) to crystalline ($Al4_{sub}$) located aluminum in dependence of the hydration ratio, we deconvoluted the signals for the Al species by Lorentz envelopes in origin software and plotted the aluminum amounts related to a total doping degree of 2 at.% for all probes against the hydration ratio (Figure 3, right). However we have to note, that the integration of solid-state ^{27}Al-NMR spectra signals does not provide reliable quantitative data. For all probes we identified amounts smaller 0.2 at.% for $Al4_{sub}$ that is in accordance with the findings of *Avadhut et al.* [25] and other authors who identified just small amounts of in ZnO solubilized aluminum by ^{27}Al-NMR [24,28,32]. With increasing hydration ratio the amount of crystalline located aluminum decreases from 0.15 at.% to 0.05 at.% Al and the amount for amorphous located aluminum increases from 1.85 at.% up to 1.95 at.% Al. So here we can show that the addition of water decreases the solubility of aluminum in ZnO. Beneath the peaks for the different known Al species we recognized and added two more peaks at around 150 ppm and 200 ppm in figure 2 (left) that are known from ^{27}Al-NMR spectra of AZO particles. The peak around 150 ppm arises due to the chemical shift anisotropy and quadrupolar interaction of Al nuclei with local electric field gradients and can be

identified as "side-spinning-band" (SSB) [33] and thus can be declared as artifact of the performed measurement. The broad peak in a range of 200 ppm can be identified as "Knight-Shift" [34] and is related to the magnetic interaction between nuclear and electronic spins and can be assigned to present conduction electrons [35]. We could clearly identify a Knight-Shift for all ^{27}Al-NMR spectra at around 200 ppm expect for AZO synthesized with the lowest hydration ratio of h=0.9 as we normalized all spectra for $Al4_{sub}$ at 81 ppm and cut the spectra at a value of 2 for the y-axis (Figure A1 in appendix). The area of the Knight-Shift is about 8-15 % for each spectrum without a tendency in dependence of the hydration ratio. The results of the ^{27}Al-NMR analysis show, that the addition of water to the precursor solution generally influences the incorporation of the dopant in ZnO. An increase of the hydration ratio results in an increase of amorphous coordinated aluminum and the appearance of the Knight-Shift for h>0.9 could be identified and is evident for an oxidic material with metallic character, and hence hints on an improved conductivity [23,25].

3.3. Electrical properties of bulk ZnO and AZO

To investigate the electrical properties of the bulk material, we measured the resistance with a two-point measurement setup as described from Pluemel [36] or Bubenhofer et al. [15]. To ensure a dense packing of the particles, the measurements were carried out with a pressure of $3.7x10^3$ bar. The results are shown in Table 2.

Table 2: Sheet-resistance of the bulk materials

Sample	Sheet resistance [Ohm*m]
ZnO	$1.28x10^5$
AZO, h=0.9	130
AZO, h=2	51
AZO, h=3	34
AZO, h=6	24
AZO, h=12	23

The incorporation of aluminum in ZnO has a big impact on the electrical properties as the sheet-resistance for doped ZnO decreases up to 4 magnitudes. So independent of the hydration ratio the incorporation of aluminium as dopant improves the electrical properties. But the influence of the hydration ratio or the resulting change of crystal-morphology influences the electrical properties. A general decrease of the resistance with increasing hydration ratio is obvious, whereas it is just significant from AZO h=0.9 to h=2 with about 80 Ohm*m. Reasons for this difference may be caused by a lower particle-to-particle contact since these particles are strongly agglomerated as we can see on the SEM photograph for AZO h=0.9. In contrast to that the difference of the sheet-resistance between AZO h=6 and 12 is negligible as we calculated a standard deviation of 1.6 Ohm*m. Even though in literature the decrease of the bulk conductivity due to minimizing the amount of grain boundaries with increasing crystal-size is mentioned, we could not find significant differences, especially when the crystal-size strongly increases from AZO h=6 with 37 nm for the [002] plane up to 59 nm for AZO h=12 as it becomes obvious from Figure 4. If we correlate the results of electrical analysis with those of the ^{27}Al-NMR analysis, it is to note that the amount of amorphous located aluminium increases with increasing hydration ratio. If we assume that the amorphously coordinated aluminum behaves as insulating "shell" as described from *Avadhut et al.* [25], it is possible that this insulating phase additionally hinders the electron transfer and counteracts an improvement of the electron-transfer by minimizing the amount of grain boundaries. But since we can't prove this hypothesis with the help of our analysis, we can just guess about it.

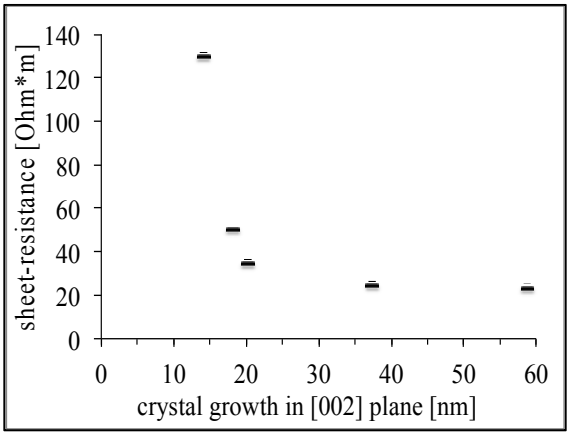

Fig. 4. Sheet-resistance of pressed AZO powders in dependence of the crystal-growth in [002] plane.

4. Conclusion

We investigated the influence of the water content and aluminum as dopant on the crystal growth of AZO nanoparticles and showed that aluminum strongly hinders the preferential growth of undoped ZnO in [002] direction. Through the addition of water the crystal-growth of AZO particles can be influenced and controlled so that spherical as well as rod-shaped particles can be obtained. The resistance of the obtained AZO particles is four magnitudes lower compared to the undoped ZnO and a slight improvement of the electrical properties with increasing crystal-size is noticeable. With the help of ^{27}Al-NMR analysis we can show that the amount of amorphous located aluminium increases if the hydration ratio increases and may act as insulating shell that reduces the electron-transfer from particle to particle. Our results present an easy way to synthesize highly crystalline and conductive particles that can be used for further investigations, for example the influence of particle sizes on the opto-electronical properties.

Acknowledgements

The national project BMBF 03X0133 “ILTIS” is supported by the Federal Ministry of Education and Research (BMBF). Special thanks for the support and great collaboration to the partners of the project.

References

[1] Fuchs, P., Hagendorfer, H., Romanyuk, Y. E., & Tiwari, A. N. (2015). Doping strategies for highly conductive Al□doped ZnO films grown from aqueous solution. *physica status solidi (a)*, *212*(1), 51-55.

[2] Castañeda, L. (2011). Present status of the development and application of transparent conductors oxide thin solid films. *Materials sciences and applications*, *2*(9), 1233-1242.

[3] Minami, T. (2005). Transparent conducting oxide semiconductors for transparent electrodes. *Semiconductor Science and Technology*, *20*(4), S.35.

[4] Stadler, A. (2012). Transparent conducting oxides—An up-to-date overview. *Materials*, *5*(4), 661-683.

[5] Liu, H., Avrutin, V., Izyumskaya, N., Özgür, Ü., & Morkoç, H. (2010). Transparent conducting oxides for electrode applications in light emitting and absorbing devices. *Superlattices and Microstructures*, *48*(5), 458-484.

[6] Gordon, R. G. (2000). Criteria for choosing transparent conductors. *MRS bulletin*, *25*(08), 52-57.

[7] Chopra, K. L., Major, S., & Pandya, D. K. (1983). Transparent conductors—A status review. *Thin solid films*, *102*(1), 1-46.

[8] Pasquarelli, R. M., Ginley, D. S., & O'Hayre, R. (2011). Solution processing of transparent conductors: from flask to film. *Chemical Society Reviews*, *40*(11), 5406-5441.

[9] Puetz, J., Dahoudi, Al, N., & Aegerter, M. A. (2004). Processing of Transparent Conducting Coatings Made With Redispersible Crystalline Nanoparticles. *Advanced Engineering Materials*, *6*(9), 733–737.

[10] Solieman, A., Aegerter, M. A. (2006). Modeling of optical and electrical properties of In2O3:Sn coatings made by various techniques. *Thin Solid Films*, *502*(1-2), 205–211.
[11] Goebbert, C., Nonninger, R., Aegerter, M. A., & Schmidt, H. (1999). Wet chemical deposition of ATO and ITO coatings using crystalline nanoparticles redispersable in solutions. *Thin Solid Films*, *351*(1-2), 79–84.
[12] Gross, M., Linse, N., Maksimenko, I., & Wellmann, P. J. (2009). Conductance enhancement mechanisms of printable nanoparticulate indium tin oxide (ITO) layers for application in organic electronic devices. *Advanced Engineering Materials*, *11*(4), 295-301.
[13] Sun, B., & Sirringhaus, H. (2005). Solution-Processed Zinc Oxide Field-Effect Transistors Based on Self-Assembly of Colloidal Nanorods. *Nano Letters*, *5*(12), 2408–2413.
[14] Wolf, N., Rydzek, M., Gerstenlauer, D., Arduini-Schuster, M., & Manara, J. (2013). Low temperature processing of redispersed tin doped indium oxide nanoparticle coatings. *Thin Solid Films*, *532*(C), 60–65.
[15] Bubenhofer, S. B., Schumacher, C. M., Koehler, F. M., Luechinger, N. A., Sotiriou, G. A., Grass, R. N., & Stark, W. J. (2012). Electrical Resistivity of Assembled Transparent Inorganic Oxide Nanoparticle Thin Layers: Influence of Silica, Insulating Impurities, and Surfactant Layer Thickness. *ACS Applied Materials & Interfaces*, *4*(5), 2664–2671.
[16] Wolf, N., Stubhan, T., Manara, J., Dyakonov, V., & Brabec, C. J. (2014). Stabilization of aluminum doped zinc oxide nanoparticle suspensions and their application in organic solar cells. *Thin Solid Films*, 564(C), 213–217.
[17] Maksimenko, I., Gross, M., Königer, T., Münstedt, H., & Wellmann, P. J. (2010). Conductivity and adhesion enhancement in low-temperature processed indium tin oxide/polymer nanocomposites. *Thin Solid Films*, 518(10), 2910–2915.
[18] Gasparro, G., Pütz, J., Ganz, D., & Aegerter, M. A. (1998). Parameters affecting the electrical conductivity of SnO 2: Sb sol–gel coatings. *Solar energy materials and solar cells*, *54*(1), 287-296.
[19] Lee, S., Jeong, S., Kim, D., Hwang, S., Jeon, M., & Moon, J. (2008). ZnO nanoparticles with controlled shapes and sizes prepared using a simple polyol synthesis. *Superlattices and Microstructures*, 43(4), 330–339.
[20] Poul, L., Ammar, S., Jouini, N., Fievet, F., & Villain, F. (2003). Synthesis of Inorganic Compounds (Metal, Oxide and Hydroxide) in Polyol Medium: A Versatile Route Related to the Sol-Gel Process. *Journal of Sol-Gel Science and Technology*, 26(1/3), 261–265.
[21] Stroppa, D. G., Montoro, L. A., Beltrán, A., Conti, T. G., da Silva, R. O., Andrés, J., Longo, E., et al. (2009). Unveiling the Chemical and Morphological Features of Sb−SnO2 Nanocrystals by the Combined Use of High-Resolution Transmission Electron Microscopy and ab Initio Surface Energy Calculations. *Journal of the American Chemical Society*, 131(40), 14544–14548.
[22] Bilecka, I., Luo, L., Djerdj, I., Rossell, M. D., Jagodič, M., Jagličić, Z., Masubuchi, Y., et al. (2011). Microwave-Assisted Nonaqueous Sol−Gel Chemistry for Highly Concentrated ZnO-Based Magnetic Semiconductor Nanocrystals. *The Journal of Physical Chemistry C*, 115(5), 1484–1495.
[23] Noriega, R., Rivnay, J., Goris, L., Kälblein, D., Klauk, H., Kern, K., Thompson, L. M., et al. (2010). Probing the electrical properties of highly-doped Al:ZnO nanowire ensembles. *Journal of Applied Physics*, 107(7), 074312.
[24] Kemmitt, T., Ingham, B., & Linklater, R. (2011). Optimization of Sol–Gel-Formed ZnO:Al Processing Parameters by Observation of Dopant Ion Location Using Solid-State 27Al NMR Spectrometry. *The Journal of Physical Chemistry C*, 115(30), 15031–15039.
[25] Avadhut, Y. S., Weber, J., Hammarberg, E., Feldmann, C., & Schmedt auf der Günne, J. (2012). Structural investigation of aluminium doped ZnO nanoparticles by solid-state NMR spectroscopy. *Physical Chemistry Chemical Physics*, 14(33), 11610.
[26] Kelchtermans, A., Elen, K., Schellens, K., Conings, B., Damm, H., Boyen, H.-G., D'Haen, J., et al. (2013). Relation between synthesis conditions, dopant position and charge carriers in aluminium-doped ZnO nanoparticles. *RSC Advances*, *3*(35), 15254.
[27] Damm, H., Adriaensens, P., De Dobbelaere, C., Capon, B., Elen, K., Drijkoningen, J., Conings, B., et al. (2014). Factors Influencing the Conductivity of Aqueous Sol(ution)–Gel-Processed Al-Doped ZnO Films. *Chemistry of Materials*, 26(20), 5839–5851.
[28] Schilling, C., Zähres, M., Mayer, C., & Winterer, M. (2014). Aluminum-doped ZnO nanoparticles: gas-phase synthesis and dopant location. *Journal of Nanoparticle Research*, *16*(7), 2506.
[29] Quartararo, J., Guelton, M., Rigole, M., Amoureux, J. P., Fernandez, C., & Grimblot, J. (1999). Sol–gel synthesis of alumina modified by phosphorus: a solid state NMR characterization study. *Journal of Materials Chemistry*, 9(10), 2637–2646.
[30] Kwak, J. H., Hu, J. Z., Kim, D. H., Szanyi, J., & Peden, C. H. (2007). Penta-coordinated Al 3+ ions as preferential nucleation sites for BaO on γ-Al 2 O 3: An ultra-high-magnetic field 27 Al MAS NMR study. *Journal of Catalysis*, *251*(1), 189-194.
[31] Liu, D., Dai, F., Tang, Z., Liu, Y., & Liu, C. (2015). The structure-directed effect of Al-based metal–organic frameworks on fabrication of alumina by thermal treatment. *Materials Research Bulletin*, *65*, 287–292.
[32] Serier, H., Gaudon, M., & MEnEtrier, M. (2009). Al-doped ZnO powdered materials: Al solubility limit and IR absorption properties. *Solid State Sciences*, *11*(7), 1192–1197.
[33] Engelhardt, G.; Michel, D. High-Resolution Solid-State NMR of Silicates and Zeolites; Wiley: New York, 1987
[34] Roberts, N., Wang, R. P., Sleight, A. W., & Warren, W. W. (1998). 27 Al and 69 Ga impurity nuclear magnetic resonance in ZnO: Al and ZnO: Ga. *Physical Review B*, *57*(10), 5734.
[35] J. J. van der Klink and H. B. Brom (2000). NMR in metals, metal particles and metal cluster compounds. *Prog. Nucl. Magn. Reson. Spectrosc*., 36, 89–201
[36] Plümel, I. (2004). Diplomarbeit: Elektronische Charakterisierung von Silizium-Nanopartikeln aus der Gasphase. https://www.uni-due.de/imperia/md/images/aglorke/abschlussarbeiten/19_diplomarbeit_pluemel.pdf

Appendix A.

A.1. ^{27}Al-NMR spectra of AZO particles

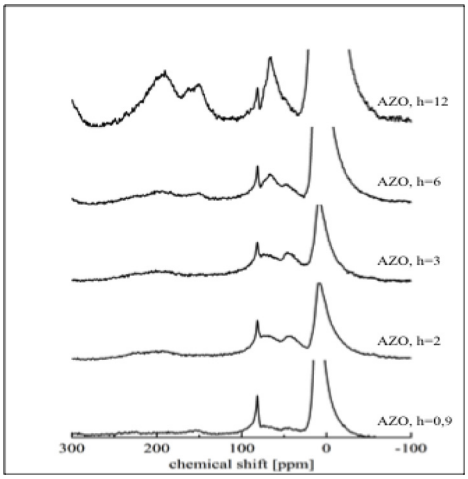

Fig. A1. ^{27}Al-NMR spectra of AZO synthesized with different hydration ratio normalized for the peak at 81 ppm and cut at a value of 2 for the y-axis.